ISSN 1029-9599, Physical Mesomechanics, 2021, Vol. 24, No. 5, pp. 503–512. © Pleiades Publishing, Ltd., 2021.
Russian Text © The Author(s), 2021, published in Fizicheskaya Mezomekhanika, 2021, Vol. 24, No. 5, pp. 5–15.

This paper is dedicated to Prof. Siegfried Schmauder who initiated and supported a long-term scientific and cultural collaboration between Tomsk and Stuttgart research teams

Evolution of Residual Stresses and Fracture in Thermomechanically Loaded Particle-Reinforced Metal Matrix Composites

R. R. Balokhonov[1]*, A. S. Kulkov[1], A. V. Zemlyanov[1], V. A. Romanova[1], E. P. Evtushenko[1], D. D. Gatiyatullina[1], and S. N. Kulkov[1†]

[1] *Institute of Strength Physics and Materials Science, Siberian Branch, Russian Academy of Sciences, Tomsk, 634055 Russia*
** e-mail: rusy@ispms.ru*

Received May 25, 2021; revised June 08, 2021; accepted June 08, 2021

Abstract—This work studies the formation and evolution of residual stresses in metal matrix composites with different volume fractions and sizes of reinforcement particles. The investigation was performed on hot-pressed samples of pure aluminum with boron and titanium carbide particles. The samples were subjected to mechanical compression tests to study their fracture behavior. Residual stresses were measured after cooling, as well as at different degrees of deformation of the composites. Some samples were subjected to electron beam processing. The phase composition and size of boron carbide particles in their recast surface layers, which were formed by recrystallization from the liquid phase during irradiation, were examined by X-ray diffraction. The cooling process followed by mechanical loading of the composites was simulated by simultaneously taking into account the fracture of the matrix and particles. The formation of residual stresses in composites with different particle volume fractions was numerically investigated.

Keywords: metal matrix composites, residual stresses, computational mesomechanics, plastic deformation, fracture

DOI: 10.1134/S1029959921050015

1. INTRODUCTION

Particle-reinforced metal matrix composites are known for their high specific strength and are widely used in mechanical engineering, energy industry, and aerospace applications. Composite coatings improve the wear resistance, corrosion resistance, and strength of the surface layers of materials. Despite the widespread use of composites, the issues concerning their strength and durability remain controversial. This is primarily due to the fact that composites have a complex multiphase structure with interfaces of various scales and with various properties. The prediction of fracture in such systems is difficult within macroscopic approaches. A solution to this problem can be found in a multilevel approach of the physical mesomechanics of materials [1, 2]. It is known that interfaces in structurally heterogeneous materials cause stress concentration, plastic strain localization, and subsequent formation of microdefects and cracks [1–6]. The local stress and strain magnitudes in the interfacial regions, among other things, depend on the difference in the thermomechanical properties of adjacent materials. The greater the difference, the higher the stresses arising at interfaces.

In recent years, there have been numerous experimental studies on the microstructure and properties of composites and coatings fabricated by various

† Deceased.

methods, e.g., laser cladding [7–11], gas dynamic spraying [12, 13], resistance seam welding [14], and solid phase sintering [15, 16]. A still unresolved question is the formation and evolution of residual stresses during fabrication and performance of composites and coatings [7, 8]. Additional studies are needed to explore the effects associated with the volume fraction, shape, size, and spatial distribution of reinforcement particles on the composite properties [12–14, 16]. A specific role in the deformation response of a coated material is played by the adhesive bond and the shape of the interface between the structural components of the composite and the coating, which are particularly determined by the deposition conditions [7, 9, 13, 10], the composition of the ceramic powder mixture [7] and the matrix [10]. The quality of the synthesized composites is also greatly affected by the changes occurring in the metal–ceramics transition zones [9]. Another fundamentally important problem is to investigate the fracture mechanisms of composite materials as well as stress and strain evolution during crack propagation both inside a ceramic particle and along the particle–matrix interface [17].

The above problems cannot be solved without studying the fundamental laws of strain and fracture localization in composites, including by numerical modeling methods with explicit consideration of structural heterogeneity. Today, such studies mainly deal with ceramic particles of a perfect round shape in a two-dimensional formulation [18, 19] or with spherical particles [20–22] in a three-dimensional formulation. Much fewer works take into account the complex shape of inclusions. For example, in [23], the deformation and fracture of SiCp/Al composite was simulated taking into account a real three-dimensional structure with several inclusions. There are also analytical estimates of how the properties of the matrix material affect the fracture behavior of reinforcement particles [24].

In our previous works, we numerically investigated the deformation and fracture of composites and coatings at different scale levels without consideration of residual stresses [4, 6], as well as the evolution of residual stresses in an elastic-plastic formulation of the problem [6, 25].

Here we study experimentally and numerically the effect of the volume fraction of reinforcement parti-

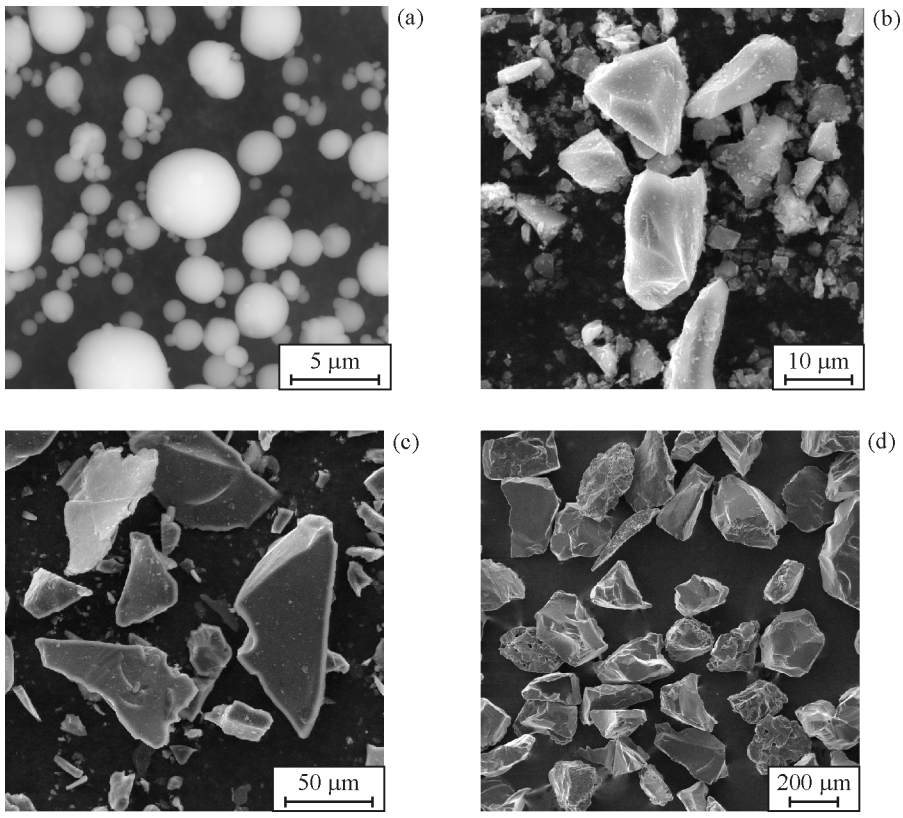

Fig. 1. Initial powders ACD-6 (a) and B_4C (b–d).

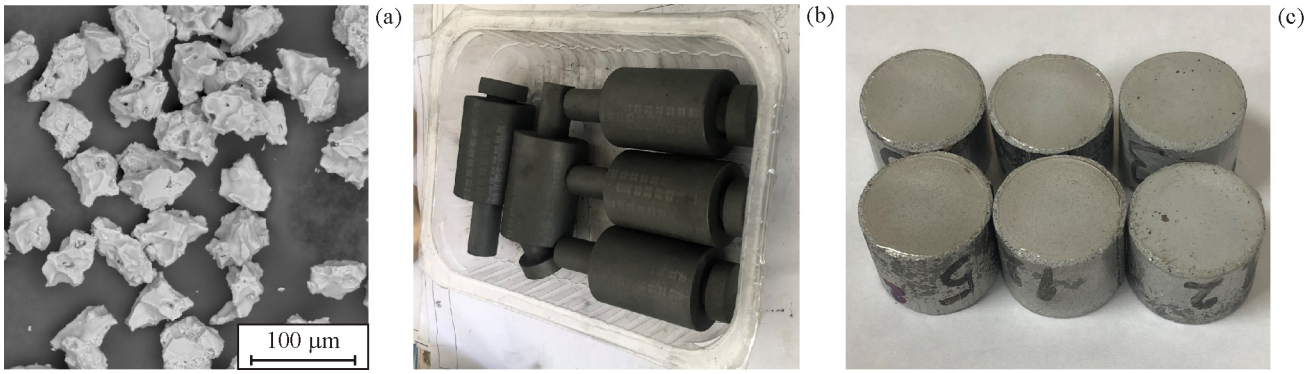

Fig. 2. TiC powder (a), dies (b), and composite samples (c).

cles on residual stress evolution and fracture behavior of thermomechanically loaded composites.

2. EXPERIMENTAL AND THEORETICAL FORMULATION OF THE PROBLEM

The investigation was performed on hot-pressed composite samples with an aluminum matrix containing boron and titanium carbide particles of different sizes and volume fractions. The size of ACD-6 aluminum powder particles ranged from 3 to 10 μm (Fig. 1a). Boron carbide inclusions B_4C were of three sizes: 10, 50–80, and 200–250 μm (Figs. 1b–1d). Titanium carbide particles were 50–80 μm in size (Fig. 2a). Graphite dies for the sintering of samples with a diameter and maximum filling depth of 15 mm are shown in Fig. 2b. Compaction was carried out in vacuum with induction heating to a temperature of 650°C under a load of 3 kN and holding for 20 min. At least 3 samples were fabricated for each particle size and volume fraction, which measured 10–12 mm in height and 15 mm in diameter (Fig. 2c). The weight of the compacted samples ranged from 3 to 6 g. Their surfaces were polished with an abrasive of up to 1 μm. Images of the composite surfaces were obtained by SEM backscattered electron imaging.

The magnitude of actual residual stresses in the aluminum matrix of the sintered composite was determined by XRD analysis. Microscopic stresses are equilibrated within individual crystals or blocks and can be either nonoriented or oriented, e.g., in the applied load direction. Microdistortions lead to X-ray line broadening that can be characterized by the quantity $\Delta d/d$, where d is the average interplanar spacing over six experiments (measured on both sides of each of the three samples) and Δd is the maximum deviation from d. X-ray diffraction patterns were obtained on a DRON-3 diffractometer using filtered copper radiation. Scanning was performed in the angular range 110°–120° with a step of 0.05° and such exposure per point as to ensure a statistical accuracy of at least 3%. This interval includes the (331) and (420) aluminum lines from which the broadening was determined using a computer program with Lorentzian line profiles of the form $1/(1+x^2)$. The instrumental broadening was taken into account by the lines of coarse-crystalline quartz in the corresponding angular range. The lattice microdistortions were determined by the formula

$$\sqrt{\langle \varepsilon^2 \rangle} = \frac{\mathrm{FWHM}}{4} \tan\theta,$$

where FWHM is the full width at half maximum of the peak in radians, and θ is the angular width of the central maximum in the diffraction pattern of the X-ray profile analyzed. The microstresses were calculated from the tabular values of the elastic modulus and Poisson's ratio for aluminum.

Mechanical tests included compression of Al-B_4C, Al-TiC samples and Brazilian tests on Al-B_4C samples. Before and after testing, the polished surface of the samples was examined by SE and BSE imaging on a Vega 3 scanning microscope. The tensile stresses in the Brazilian test were calculated by the formula $\sigma = F/(\pi R t)$, where F is the breaking load, and R, t are the radius and thickness of the sample.

The effect of the volume fraction of ceramic inclusions on the residual stress magnitude was studied with aluminum and boron carbide particles of size 50 μm. The B_4C volume fraction was 1, 3, 6, 10, 12, and 20%. The residual stresses were investigated in samples with a B_4C content of 1, 10, and 20%. The mechanical testing of composite samples, metallographic analysis, and residual stress measurements were performed at successive loading, unloading, and reloading to 3, 7, 15, 25, and 50% strains. Residual

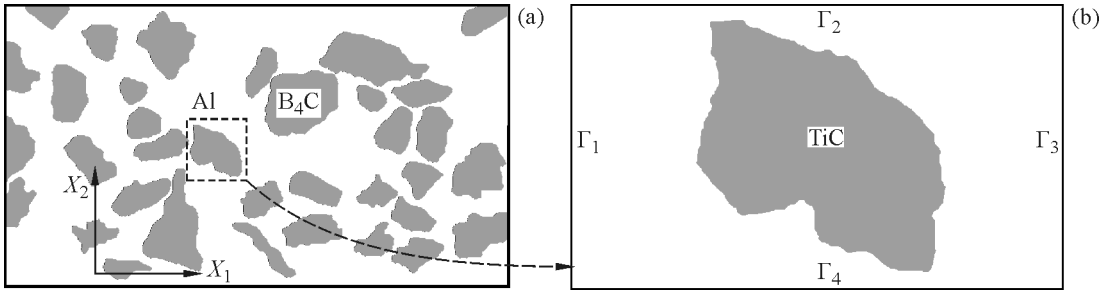

Fig. 3. Model structure of a composite with a large volume fraction of particles (a) and a lower-scale structure with a single inclusion (b).

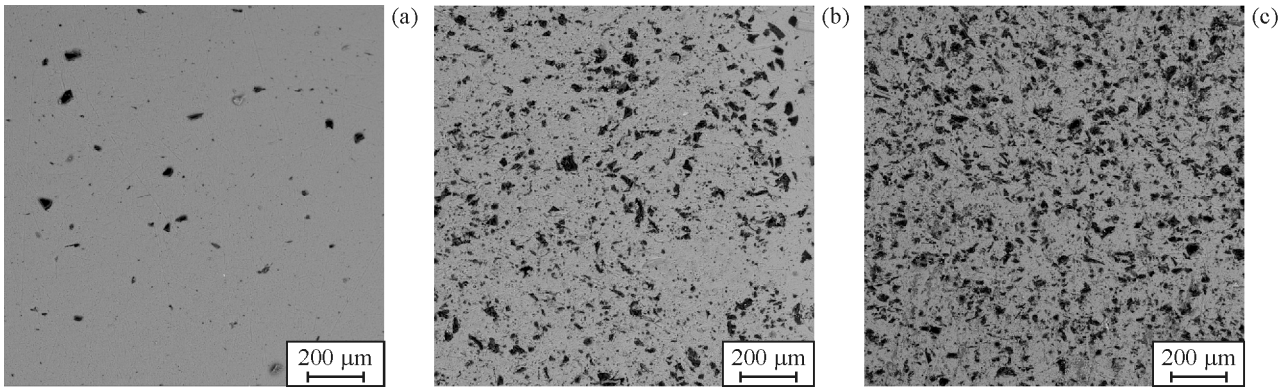

Fig. 4. Al-B_4C composites with different volume fractions of particles: 1 (a), 10 (b) and 20% (c). Scanning electron microscopy.

stresses were measured on the lateral surface of the sample, without additional surface processing after compression.

The structure and residual stresses were also investigated in the Al-B_4C metal matrix composite manufactured by solid phase sintering with subsequent electron beam surface processing.

The structure of the recast composite layer in numerical simulations corresponded to the experimentally observed one (Fig. 3). The volume fraction of particles was varied in the calculations.

The dynamic boundary value problem of structural deformation during cooling followed by compression was solved numerically using ABAQUS finite element package for plane stress conditions. It includes the momentum and mass conservation laws, equations for strain rates (1), and constitutive equations (2):

$$\sigma_{ij,j} = \rho\ddot{u}_i,\ \dot{\rho}/\rho = -\dot{\varepsilon}_{kk},\ \dot{\varepsilon}_{ij} = (\dot{u}_{i,j} + \dot{u}_{j,i})/2, \quad (1)$$

$$\dot{\sigma}_{ij} = -\dot{P}\delta_{ij} + \dot{S}_{ij} = K(\dot{\varepsilon}_{kk} - 3\alpha\dot{T})\delta_{ij} + 2\mu(\dot{\varepsilon}_{ij} - \dot{\varepsilon}_{kk}\delta_{ij}/3 - \dot{\varepsilon}^{\mathrm{p}}_{ij}), \quad (2)$$

where u_i is the displacement vector, σ_{ij}, ε_{ij} and $\varepsilon^{\mathrm{p}}_{ij}$ are the stress, total strain and plastic strain tensors, S_{ij} is the deviatoric stress tensor, P is the pressure, δ_{ij} is the Kronecker delta, K and μ are the bulk compression and shear moduli, ρ is the density, α is the thermal expansion coefficient, the dot and comma denote the time and coordinate derivatives, respectively.

The inelastic behavior of the aluminum matrix is described using the plastic flow rule $\dot{\varepsilon}^{\mathrm{p}}_{ij} = \dot{\lambda}S_{ij}$ associated with the yield condition of the form $\sigma_{\mathrm{eq}} - \sigma_0(\varepsilon^{\mathrm{p}}_{\mathrm{eq}}) = 0$, where σ_{eq} and $\varepsilon^{\mathrm{p}}_{\mathrm{eq}}$ are the equivalent stress and accumulated equivalent plastic strain, and σ_0 is the isotropic hardening function.

Table 1. Experimental residual stress values of the aluminum matrix at different volume fractions and sizes of ceramic particles

Volume fraction of B_4C particles, %	Particle size, μm	Residual stresses, MPa
0	–	26
3	200	27.4
6	200	28.7
12	200	32.0
20	200	35
20	50	38
20	10	30

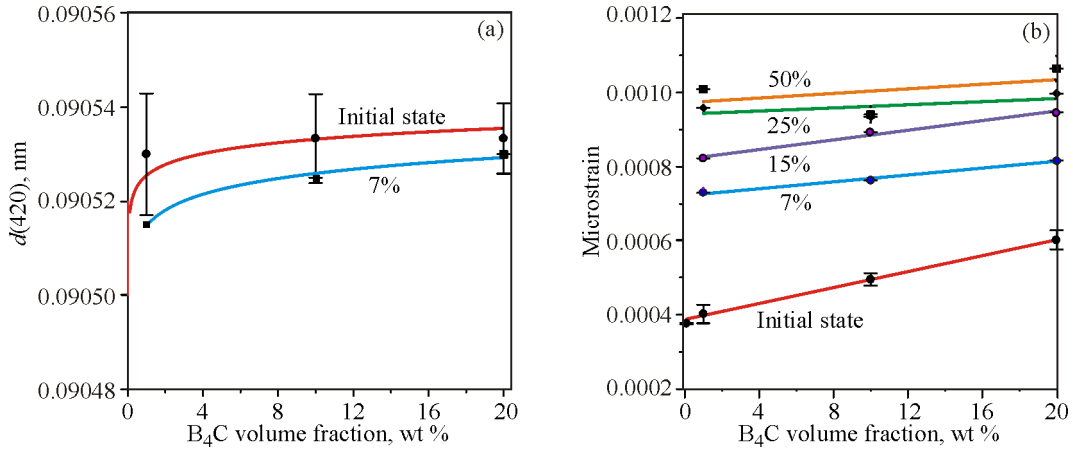

Fig. 5. Dependence of interplanar spacing on boron carbide content after cooling (•) and at 7% compression of the composite (■) (a), and lattice microstrains at various degrees of compression (b) (color online).

The cracking of ceramic particles is analyzed using a Huber–Mises criterion that takes into account crack initiation in bulk tensile regions:

$$\sigma_{eq} = C_{ten} \text{ at } \varepsilon_{kk} > 0, \quad (3)$$

where C_{ten} is the tensile strength.

Local areas of the metal matrix are assumed to be fractured if the accumulated equivalent plastic strain exceeded a critical value.

The boundary conditions on the surfaces Γ_1 and Γ_3 simulate the uniaxial tension/compression of a mesovolume in direction 1, and those on Γ_2 and Γ_4 correspond to the free surface conditions (Fig. 3). Cooling of the sintered sample is simulated by a uniform linear decrease in temperature (the same at all points of the sample) from 350°C to a room temperature of 23°C.

3. RESIDUAL STRESS GENERATION AND FRACTURE OF PARTICLES UNDER THERMOMECHANICAL LOADING OF THE COMPOSITE

The sintered aluminum structures with different volume fractions of boron carbide particles are shown in Fig. 4. Results of residual stress measurements after sintering of the composites are summarized in Table 1. As one can see, the average stresses in the matrix increase with increasing volume fraction of particles and decreasing particle size. For fine particles, the average residual stresses decrease.

Residual stress measurements after cooling and cyclic compression of sintered composites with different particle volume fractions to different strains showed the following. First of all, we notice a very good agreement of the aluminum interplanar spacing

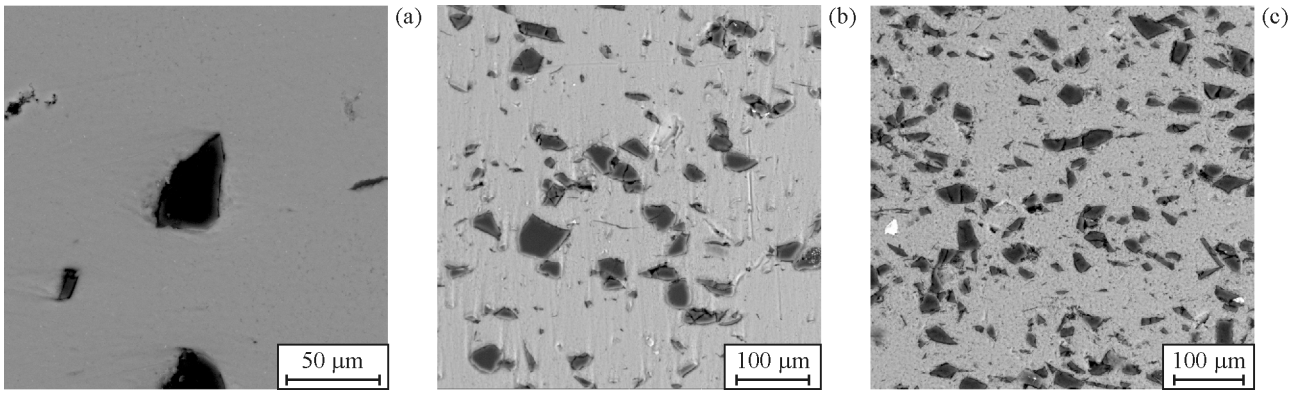

Fig. 6. Al-B_4C composites with a volume fraction of boron carbide particles: 1 (a), 10 (b) and 20% (c), strained to 7%. Scanning electron microscopy.

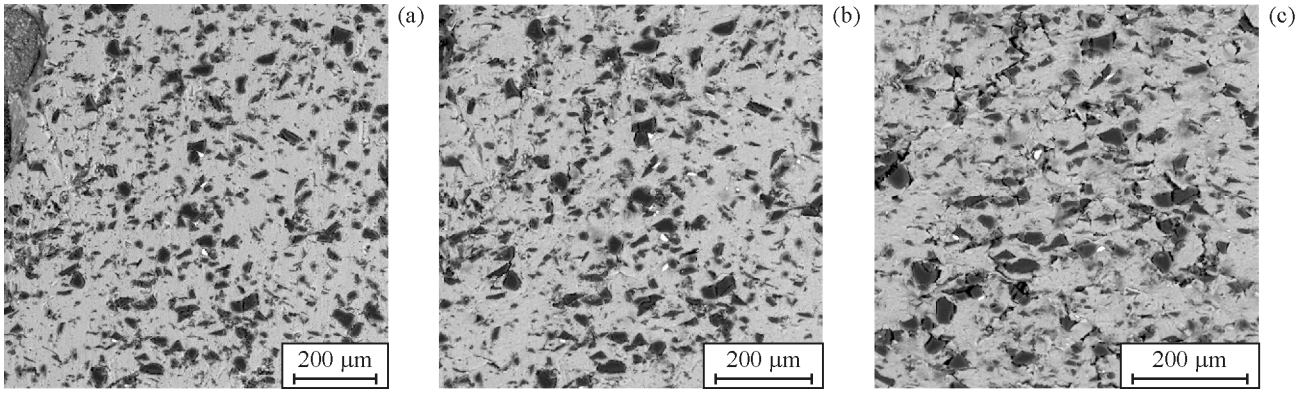

Fig. 7. Al-B_4C composites with a 20% volume fraction of boron carbide particles, strained to 2 (a), 15 (b) and 50% (c). Scanning electron microscopy.

parameter with the tabular value (ASTM 4-787). The difference is ±0.000005 nm, which indicates the reliability of the measurements. The addition of boron carbide leads to a slight increase in the parameter to about 0.00002 nm (Fig. 5). Since the Bragg–Brentano focusing scheme was used, the increase means that the addition of boron carbide causes the generation of macroscopic (compressive) stresses. Figure 5a (square symbols) shows the change in this parameter after macrodeformation of the hot-pressed sample to 7% strain. The parameter $d(420)$ slightly decreases by about 0.00001 nm, indicating macrostress growth under macroscopic loading. The macrodeformation of the sample causes a noticeable broadening of the X-ray diffraction line. This broadening is equivalent to the generation of microscopic residual stresses of the order of 30 MPa (Fig. 5b). With further sample deformation to 50%, the dislocation density increases, and the increase in the microscopic residual stresses slows down. In this case, the residual stress magnitude at large strains weakly depends on the boron carbide content.

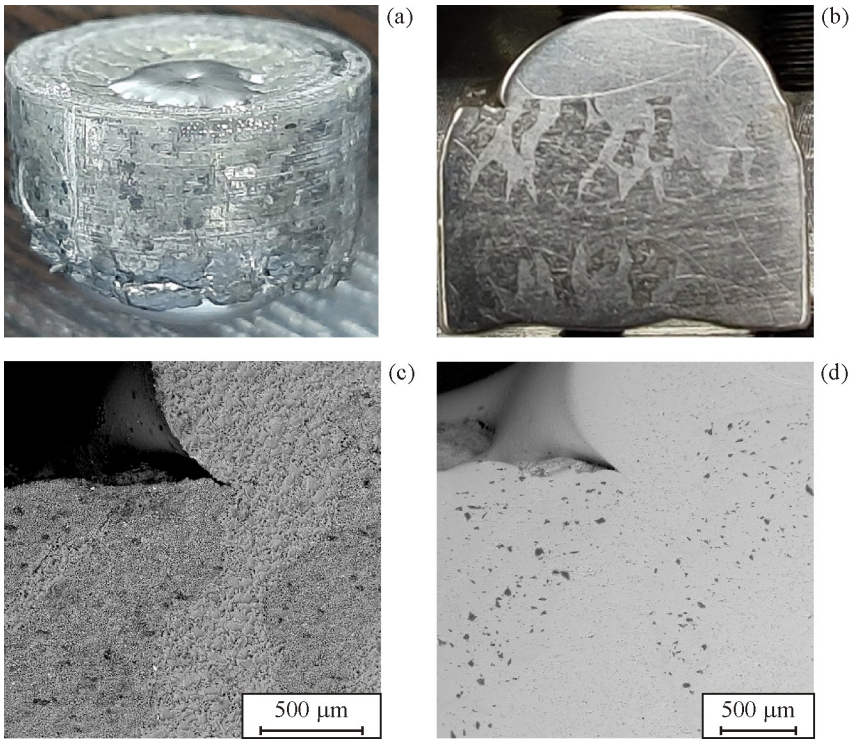

Fig. 8. Sintered Al-10% B_4C composite sample with electron-beam recast surface (a), its cross-sectional view (b), and SEM-BSE images of unpolished (c) and polished (d) lateral face.

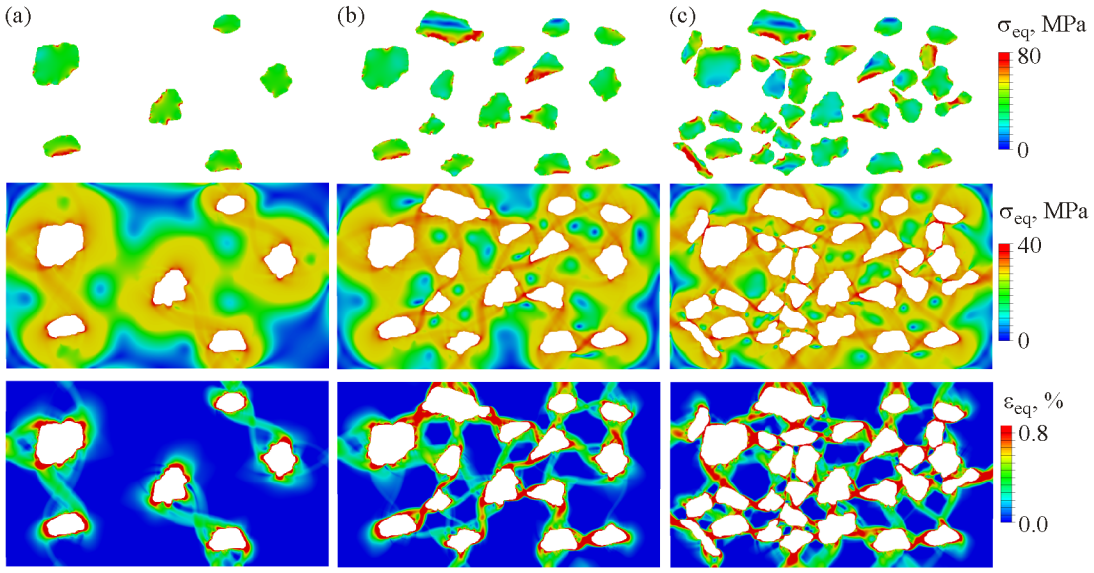

Fig. 9. Calculated equivalent stress and plastic strain distributions in cooled aluminum samples with different volume fractions of boron carbide particles: 8 (a), 16 (b) and 27% (c) (color online).

Samples with different volume fractions of boron carbide particles were successively compressed to 2–50% strains. After each stage of compression, the surface was examined by electron microscopy (Figs. 6 and 7). The examination revealed that cracking begins in the sample already at 7% strain, primarily at the particle–matrix interfaces and inside particles, and progresses mainly in the compression axis direction. With increasing volume fraction of boron carbide, the particle fracture is more pronounced.

Localized plastic flow in the matrix can be observed already from 15% strain of the composite. New cracks are formed in the particles and existing cracks open. With further deformation, visible fracture regions appear in the matrix at an angle of 45° to or along the compression axis. Some cracks stop at the particles and do not propagate further.

Figure 8 shows an electron beam irradiated hot-pressed sample of Al-10% B_4C composite. As a result of irradiation, the upper layer of the composite melts and aluminum is squeezed out along the "streamlines" in the bulk of the sample. The material in these regions has the lowest porosity and there are no large boron carbide particles, while the surrounding material depleted in the aluminum binder has the highest porosity. Such a redistribution of aluminum is due to the low wettability (high contact angle) of boron carbide with aluminum, which is squeezed onto the surface in the form of a drop as a result of electron beam irradiation. This factor is not decisive

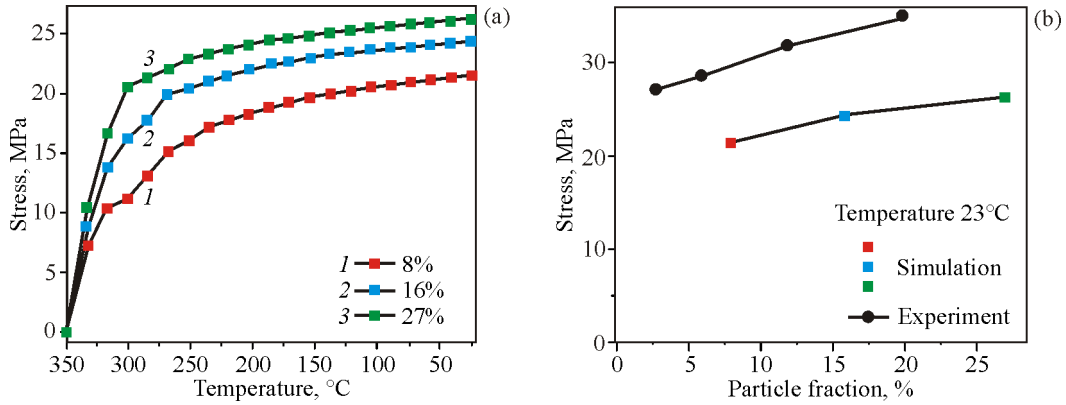

Fig. 10. Evolution of average equivalent stresses in the matrix during cooling of composites with different volume fractions of boron carbide particles (a), and residual stresses in the matrix after cooling in comparison with experiment (b) (color online).

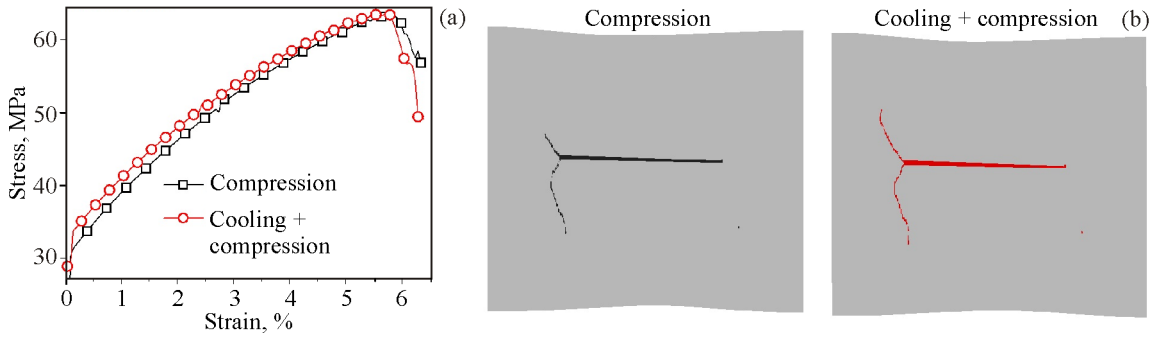

Fig. 11. Numerical flow curves of aluminum–titanium carbide composite (a) and fracture patterns at 6.3% compression from the initial state and after cooling (b) (color online).

in the case of hot pressing because the process takes place in the solid state, and when the liquid phase appears it is displaced from the bulk of the material. Residual microstrain measurements in the molten aluminum layer without large boron carbide particles and in the middle part of the sample yielded values of 6.6×10^{-4} and 6.4×10^{-4}, which are 10% higher than microstrains in the unirradiated sintered composite (Fig. 5b). X-ray studies of the phase composition of the molten drop showed that its central part is significantly depleted in boron carbide (almost by a factor of 2), and the particles have a much smaller size compared to the volume of the hot-pressed composite. The detected X-ray line broadening of boroncarbide indicates recrystallization from the liquid phase during electron beam processing, and the recrystallization took place under nonisothermal conditions.

Numerical simulations were performed to solve two types of problems: cooling of model composite structures to room temperature with subsequent compression, and compression of structures from the initial undeformed state (Figs. 9–12).

As a result of the composite cooling, stresses concentrate at the matrix–particle interfaces due to the difference in the thermal expansion coefficients between aluminum and boron carbide, both in elastic ceramic particles and in the plastic matrix. The final residual stress and strain distributions after cooling of the aluminum–boron carbide composite are shown in Fig. 9 for different volume fractions of ceramic particles. It was found that the stresses in the particles are more than 2 times higher than in the matrix. Residual stress zones in the matrix appear as concentric circular areas around each particle. The stresses are maximum near the particle and decrease with distance from the interface. The size of these zones is on the order of the particle diameter. The boundaries of the zones are clearly defined. Stress concentrations cause plastic flow in the matrix around the particles. As can be seen from Fig. 9, particles interact with

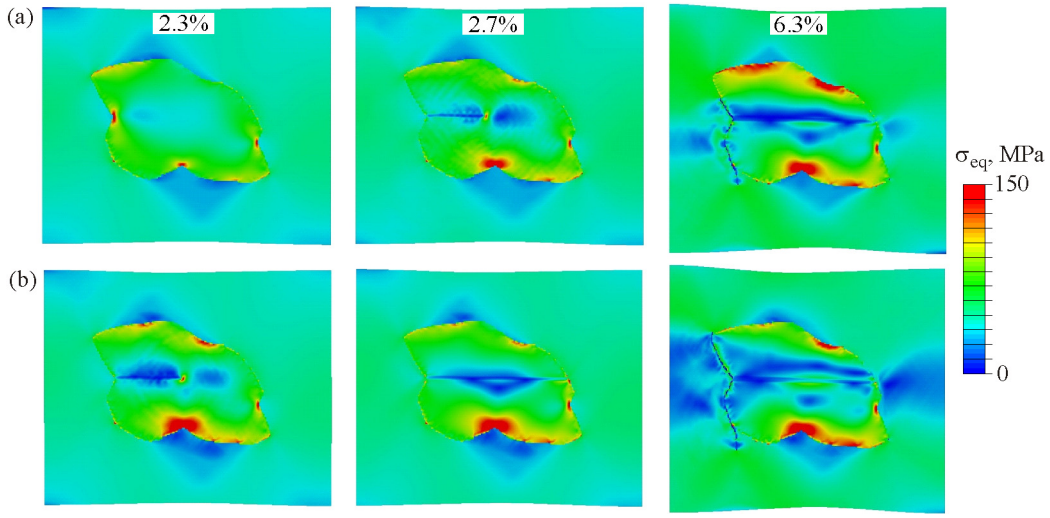

Fig. 12. Calculated equivalent stresses at different degrees of compression of aluminum–titanium carbide composite from the initial state (a) and after cooling (b). Corresponding states on the flow curve are shown in Fig. 11a (color online).

each other already at a particle volume fraction of 8%. The circular residual stress zones induced by individual particles overlap and form intersecting stress and strain localization bands. The higher the fraction of particles, the greater their influence on each other and, accordingly, the larger the number of zones of concentrated residual stresses and localized plastic strains in the matrix (Figs. 6, 9, and 10).

Figure 10 illustrates changes in the equivalent stresses averaged over the matrix volume during cooling of sintered composites with different volume fractions of boron carbide particles. The nonuniform accumulation of residual stresses at the initial stages of cooling in the temperature range of 350–250°C is associated with the sequential onset and development of localized plastic flow around individual irregularly shaped boron carbide particles. The less the particles interact with each other, the more active this process is (Fig. 10a, volume fraction 8%). Further when the entire matrix around the particles is involved in the plastic flow, the averaged stresses increase monotonically. The final states at the temperature 23°C were obtained by averaging the stress fields in the matrix illustrated in Fig. 9 and are shown in Fig. 10b in comparison with experiment (Table 1). The numerical and experimental curves agree qualitatively. The lower level of residual stresses in the calculations in comparison with the experiment is due to the fact that the defect structure of the aluminum matrix is not taken into account in the simulation. We consider only the contribution associated with the effect of carbide particles.

The deformation and fracture of aluminum–titanium carbide composite were simulated on a sample containing a single particle. It was shown that for the given structure and properties of the materials residual stresses have little effect on the strength of the composite (Fig. 11). In the case when residual stresses are taken into account, cracks in both the particle and then in the matrix are initiated earlier than in the case when the composite is compressed from the initial state (Fig. 12). Cracks in the particle propagate along the compression direction. With increasing degree of compression, fracture originates in the aluminum matrix in the same place where the crack was first initiated in the particle, and propagates along the particle–matrix interface. However, fracture propagation has little effect on the integral flow curves of the materials. Moreover, preliminary plastic deformation of the matrix during cooling strengthens aluminum, and the current deformation resistance during subsequent compression turns out to be slightly higher than when residual stresses are not taken into account (Fig. 11a).

4. CONCLUSIONS

The study was carried out on hot-pressed metal matrix composite samples with reinforcement boron and titanium carbide particles of different sizes and volume fractions. The samples were subjected to mechanical compression tests and deformed to various strains with residual stress measurements. X-ray diffraction analysis was used to examine the phase composition and size of boron carbide particles in the molten surface layers of the composite samples, which were formed by recrystallization from the liquid phase during electron beam processing. The generation of residual stresses in composites with different particle volume fractions and the effect of residual stresses on crack initiation and growth, both in ceramic particles and in the metal matrix, were investigated numerically. The simulation results agree with experiment and suggest the following.

Cracks in ceramic particles propagate along the compression direction and perpendicular to the tensile axis. As the volume fraction of boron carbide increases, the fracture process is enhanced.

An increase in the volume fraction of particles and their size reduction lead to an increase in residual stresses in the matrix of the fabricated composites. At large strains the residual stress magnitude weakly depends on the boron carbide content. The regions of the composite recrystallized during electron beam processing are depleted in boron carbide, and the particles are smaller in size as compared to the volume of the hot-pressed composite. Residual stresses have little effect on the strength of pure aluminum–titanium carbide composite during compression, only slightly increasing the current deformation resistance.

FUNDING

The work was supported by the Russian Science Foundation, Grant No. 18-19-00273, https://rscf.ru/en/project/18-19-00273/. Fracture model (3) used in this study was developed as part of the government statement of work for ISPMS SB RAS, Research Topic No. FWRW-2021-0002.

REFERENCES

1. *Physical Mesomechanics of Heterogeneous Media and Computer-Aided Design of Materials*, Panin, V.E., Ed., Cambridge: Cambridge International Science Publishing, 1998.

2. *Multiscale Materials Modeling: Approaches to Full Multiscaling*, Schmauder, S. and Schäfer, I., Eds., Berlin: De Gruyter, 2016.
3. Romanova, V.A., Soppa, E., Schmauder, S., and Balokhonov, R.R., Mesomechanical Analysis of the Elasto-Plastic Behavior of a 3D Composite-Structure under Tension, *Comput. Mech*., 2005, vol. 36, pp. 475–483.
4. Balokhonov, R.R., Romanova, V.A., Schmauder, S., and Emelianova, E.S., A Numerical Study of Plastic Strain Localization and Fracture Across Multiple Spatial Scales in Materials with Metal-Matrix Composite Coatings, *Theor. Appl. Fract. Mech*., 2019, vol. 101, pp. 342–355.
5. Moiseenko, D.D., Maksimov, P.V., Panin, S.V., Schmauder, S., Panin, V.E., Babich, D.S., Berto, F., Vinogradov, A.Yu., and Brückner-Foit, A., Recrystallization at Crack Surfaces as a Specific Fracture Mechanism at Elevated Temperatures—Cellular Automata Simulation, *Phys. Mesomech*., 2020, vol. 23, no. 1, pp. 1–12. https://doi.org/10.1134/S1029959920010014
6. Balokhonov, R.R., Evtushenko, E.P., Romanova, V.A., Schwab, E.A., Bakeev, R.A., Emelyanova, E.S., Zinovyeva, O.S., Zinovyev, A.V., and Sergeev, M.V., Formation of Bulk Tensile Regions in Metal Matrix Composites and Coatings under Uniaxial and Multiaxial Compression, *Phys. Mesomech*., 2020, vol. 23, no. 2, pp. 135–146. https://doi.org/10.1134/S1029959920020058
7. Muvvala, G., Karmakar, D.P., and Nath, A.K., In-Process Detection of Microstructural Changes in Laser Cladding of In-Situ Inconel 718/TiC Metal Matrix Composite Coating, *J. Alloys Compd.*, 2018, vol. 740, pp. 545–558.
8. Tao, Y.-F., Li, J., Lv, Y.-H., and Hu, L.-F., Effect of Heat Treatment on Residual Stress and Wear Behaviors of the TiNi/Ti_2Ni Based Laser Cladding Composite Coatings, *Opt. Laser Tech*., 2017, vol. 97, pp. 379–389.
9. Liu, D., Hu, P., and Min, G., Interfacial Reaction in Cast WC Particulate Reinforced Titanium Metal Matrix Composites Coating Produced by Laser Processing, *Opt. Laser Tech*., 2015, vol. 69, pp. 180–186.
10. Riquelme, A., Escalera-Rodríguez, M.D., Rodrigo, P., Otero, E., and Rams, J., Effect of Alloy Elements Added on Microstructure and Hardening of Al/SiC Laser Clad Coatings, *J. Alloys Compd.*, 2017, vol. 727, pp. 671–682.
11. Verdi, D., Garrido, M.A., Múnez, C.J., and Poza, P., Influence of Exposure at High Temperature on the Local Scratch Mechanisms in Laser Cladded Inconel 625-Base Metal Matrix Composite Coatings, *J. Alloys Compd.*, 2018, vol. 733, pp. 69–81.
12. Peat, T., Galloway, A., Toumpis, A., McNutt, P., and Iqbal, N., The Erosion Performance of Particle Reinforced Metal Matrix Composite Coatings Produced by Co-Deposition Cold Gas Dynamic Spraying, *Appl. Surf. Sci*., 2017, vol. 396, pp. 1623–1634.
13. Lee, Y.T.R., Ashrafizadeh, H., Fisher, G., and McDonald, A., Effect of Type of Reinforcing Particles on the Deposition Efficiency and Wear Resistance of Low-Pressure Cold-Sprayed Metal Matrix Composite Coatings, *Surf. Coat. Tech*., 2017, vol. 324, pp. 190–200.
14. Wang, W., Zengb, X., Lia, Y., Wang, D., Liu, Y., Yamaguchi, T., Nishio, K., and Cao, J., Fabrication, Microstructure, and Wear Performance of WC-Fe Composite/Metal Coating Fabricated by Resistance Seam Welding, *Appl. Surf. Sci*., 2018, vol. 439, pp. 468–474.
15. Cabezas-Villa, J.L., Olmos, L., Vergara-Hernández, H.J., Jiménez, O., Garnica, P., Bouvard, D., and Flores, M., Constrained Sintering and Wear Properties of Cu−WC Composite Coatings, *Trans. Nonferr. Met. Soc. China*, 2017, vol. 27, pp. 2214−2224.
16. Pramanik, Basak, A.K., Fracture and Fatigue Life of Al-Based MMCs Machined at Different Conditions, *Eng. Fract. Mech*., 2018, vol. 191, pp. 33–45.
17. Asif Iqbal, A.K.M., Chen, S., Arai, Y., and Araki, W., Study on Stress Evolution in SiC Particles during Crack Propagation in Cast Hybrid Metal Matrix Composites Using Raman Spectroscopy, *Eng. Failure Analysis*, 2015, vol. 52, pp. 109–115.
18. Josyula, S.K. and Narala, S.K.R., Study of TiC Particle Distribution in Al-MMCs Using Finite Element Modeling, *Int. J. Mech. Sci*., 2018, vol. 141, pp. 341–358.
19. Wang, D., Shanthraj, P., Springer, H., and Raabe, D., Particle-Induced Damage in Fe–TiB_2 High Stiffness Metal Matrix Composite Steels, *Mater. Design*, 2018, vol. 160, pp. 557–571.
20. Shakoor, M., Bernacki, M., and Bouchard, P.-O., Ductile Fracture of a Metal Matrix Composite Studied Using 3D Numerical Modeling of Void Nucleation and Coalescence, *Eng. Fract. Mech*., 2018, vol. 189, pp. 110–132.
21. Jarząbek, D.M., Dziekoński, C., Dera, W., Chrzanowska, J., and Wojciechowski, T., Influence of Cu Coating of SiC Particles on Mechanical Properties of Ni/SiC Co-Electrodeposited Composites, *Ceramics Int*., 2018, vol. 44, pp. 21750–21758.
22. Ma, L., Huang, Ch., Dolman, K., Tang, X., Yang, J., Shi, Zh., and Liu, Zh.-Sh., A Method to Calculate the Bulk Hardness of Metal Matrix Composite Using Hadfield Steel Reinforced with Niobium Carbide Particles as an Example, *Mech. Mater*., 2017, vol. 112, pp. 154–162.
23. Zhang, J.F., Zhang, X.X., Wang, Q.Z., Xiao, B.L., and Ma, Z.Y., Simulations of Deformation and Damage Processes of SiCp/Al Composites during Tension, *J. Mater. Sci. Tech*., 2018, vol. 34, pp. 627–634.
24. Li, Y., Cao, J., and Williams, C., Competing Failure Mechanisms in Metal Matrix Composites and Their Effects on Fracture Toughness, *Materialia*, 2019. https://doi.org/10.1016/j.mtla.2019.100238
25. Balokhonov, R., Romanova, V., Schwab, E., Zemlianov, A., and Evtushenko, E., Computational Microstructure-Based Analysis of Residual Stress Evolution in Metal-Matrix Composite Materials during Thermomechanical Loading, *Facta Univ. Mech. Eng*., 2021. https://doi.org/10.22190/FUME201228011B